

## Gaussian Beam Analysis of Temporal Waveform of Focused Terahertz Pulses

Toshiaki HATTORI\*, Rakchanok RUNGSAWANG, Keisuke OHTA and Keiji TUKAMOTO

*Institute of Applied Physics, University of Tsukuba, 1-1-1 Tennodai, Tsukuba 305-8573, Japan*

(Received December 11, 2001; revised manuscript received April 17, 2002; accepted for publication May 13, 2002)

Temporal waveform transformation of terahertz electromagnetic pulses near the focus was studied by experiments and simulations. The terahertz pulses were generated by a large-aperture photoconductive emitter, and focused by an off-axis parabolic mirror. Changes of the temporal waveforms due to the propagation near the focus were measured using the electro-optic sampling method. Experimentally observed waveforms were compared with those of simulations based on the Gaussian beam model, and good agreement between them was obtained. A simple analytical expression describing the amplitude and the temporal shape of the focused THz waveform was also derived. [DOI: 10.1143/JJAP.41.5198]

KEYWORDS: terahertz, femtosecond, large aperture, photoconductive antenna, Gaussian beam

### 1. Introduction

Generation of giant terahertz electromagnetic pulses has become possible by the recent development of the generation technique using large-aperture biased photoconductive antennas excited by femtosecond optical pulses. An electric field of focused THz pulses on the order of 10 kV/cm has been reported.<sup>1–3</sup> Since almost monocycle terahertz pulses generated using ultrashort optical pulses have a very broad power spectrum extending from dc to a few THz, and the wavelength of a significant spectral portion is longer than the source or other optical elements, the temporal waveform of the pulse is dependent on the position, and changes significantly via propagation and focusing processes.<sup>4</sup> The waveform is affected even by propagation through a sub-centimeter-size metal aperture, where development of a negative tail has been observed after the main peak of a half-cycle waveform.<sup>5</sup> To achieve a high electric field, it is important to characterize the waveform transformation and change in the absolute peak field of the THz pulses during propagation through free space and focusing optics. Near-field propagation of THz pulses has been studied by numerically calculating the electric field using diffraction theories.<sup>6,7</sup> Since the large-aperture photoconductive antenna used in the present study has an area of  $3 \times 3 \text{ cm}^2$ , propagation of the THz pulses should essentially be treated based on near-field optics. The only exceptions are the pulse characteristics around the focus. The characteristics of the field around the focus are essentially those of the far field except that the magnitude of the field is much larger. Since in most applications of THz pulses generated from large-aperture antennas the field at the focus is utilized, our primary interest lies in the properties of the THz pulses around the focus.

Therefore, in the present study, we focused on the transformation of the temporal waveforms of the pulses around the focus. Studies on the spatial profiles of the THz field distribution around the focus will be reported in a separate paper.<sup>8</sup> The waveforms were observed experimentally using the electro-optic method, and the results were compared with those obtained by simulations based on the Gaussian beam theory.<sup>1</sup> The Gaussian beam method is simpler than the numerical method using the diffraction integral,<sup>6</sup> and is expected to be valid for the description of

the THz waveform transformation around the focus since it can satisfactorily describe propagation of optical beams in the far-field region.

### 2. Experiments

Time-resolved THz field measurements by the electro-optic (EO) method<sup>9</sup> were performed to observe the THz waveforms around the focus using the experimental setup shown in Fig. 1, which is similar to that described in the previous paper.<sup>3</sup> The emitter of THz radiation was a nondoped semi-insulating GaAs wafer with a (100) surface. The diameter and thickness of the wafer were 50 mm and 350  $\mu\text{m}$ , respectively. Two aluminum electrodes were mechanically brought in contact with the wafer with an intergap spacing of 30 mm. A pulsed electrical voltage of 12 kV was applied to the electrodes. The duration and the repetition rate of the voltage pulse were 1  $\mu\text{s}$  and 1 kHz, respectively.

The light source used in the experiment was regeneratively amplified femtosecond Ti:sapphire laser pulses (Spitfire, Spectra Physics). The pulse width, pulse energy,

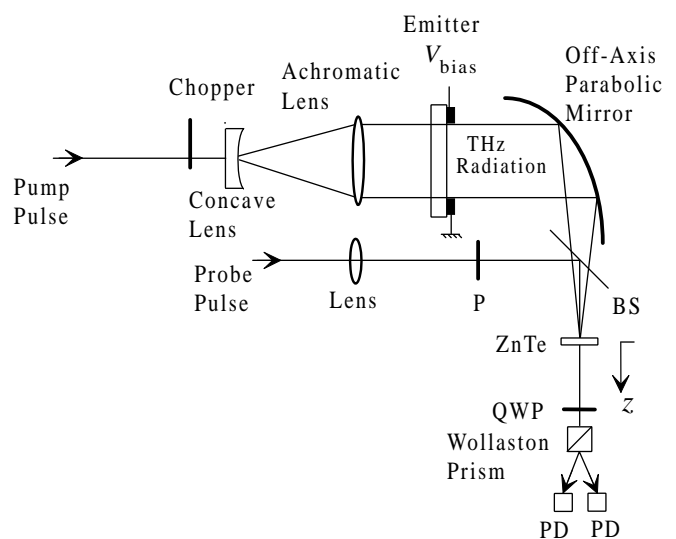


Fig. 1. Schematic of the experimental setup of the electro-optic sampling measurement of waveforms of THz radiation emitted by a large-aperture photoconductive antenna. The ZnTe crystal was moved along the propagation axis,  $z$ . The origin of the  $z$  axis was taken at the focus of the parabolic mirror. BS: pellicle beamsplitter, P: polarizer, PD: photodiode, and QWP: quarter-wave plate.

\*E-mail address: hattori@bk.tsukuba.ac.jp

wavelength, and repetition rate of the output of the amplifier were approximately 150 fs, 800  $\mu\text{J}$ , 800 nm, and 1 kHz, respectively. A major portion of the amplifier output was used to pump the GaAs emitter. A small portion was split off and used as a probe beam. The pump beam was attenuated by a filter, and chopped at 500 Hz by a mechanical chopper, which was synchronized to the amplifier output. The beam was expanded and collimated by a combination of a convex lens and an achromatic lens with focal lengths of 40 and 170 mm, respectively, and incident at the center of the intergap area of 900  $\text{mm}^2$  of the emitter synchronously with the high applied voltage. The pump pulse energy was 9.5  $\mu\text{J}$ . The spatial distribution of the fluence of the pump pulse on the emitter was measured using a knife-edge experiment, and it was found to be nearly Gaussian. The  $1/e$  radius obtained was 9.2 mm. The pump fluence at the center of the emitter is calculated to be 3.6  $\mu\text{J}/\text{cm}^2$  using these values.

THz radiation generated from the emitter in the transmission direction was focused by an off-axis parabolic mirror onto a 1.33-mm-thick  $\langle 110 \rangle$  ZnTe crystal. The focal length of the off-axis parabolic mirror was 152.4 mm. The parabolic mirror was circular when seen from the direction of the emitter, and its diameter was 50.8 mm. The distance between the GaAs wafer and the parabolic mirror was 83 mm. The ZnTe crystal was oriented such that the (001) direction was parallel to the polarization of the THz radiation. The crystal was placed in a metal holder, and covered by a 1-mm-thick metal plate on the side where the THz beam was incident. The plate had a square window of 8 mm  $\times$  8 mm size. The probe pulse was set to be linearly polarized at 45° from the THz polarization.

The phase difference,  $\Delta\theta$ , between light with the THz polarization direction and the orthogonal direction is expressed as

$$\Delta\theta = \frac{\pi d r_{41} n_0^3}{\lambda} E_{\text{THz}}(t). \quad (1)$$

Here,  $\lambda$  is the wavelength of the probe light, and  $d$ ,  $r_{41}$ , and  $n_0$  are the thickness, the EO constant, and the refractive index of the ZnTe crystal, respectively. Literature values of  $r_{41} = 4.0 \text{ pm/V}$  and  $n_0 = 2.85$  were used for these parameters in the calculation of the THz field from the experimental data.<sup>10,11)</sup>

Probe pulses were reflected by a pellicle beamsplitter and loosely focused on the ZnTe crystal by a lens in a collinear geometry with the THz radiation. Probe pulses which passed through the ZnTe crystal propagated through a quarter-wave plate, and the polarization change due to the EO effect was detected by a combination of a Wollaston prism and a pair of Si photodiodes. The difference of the output of the two photodiodes was sent to a lock-in amplifier, and a 500-Hz component was recorded. In order to observe the change in the waveform around the focus, the ZnTe crystal was translated in the direction of the beam propagation. This direction was taken as the  $z$  axis, and the origin was located at the geometrical focus of the off-axis parabolic mirror. The ZnTe crystal was moved from the focus ( $z = 0 \text{ mm}$ ) to  $z = 50 \text{ mm}$ . THz waveforms at positions closer to the parabolic mirror than the focus could not be measured because of geometrical contact between optical elements and holders.

### 3. Theoretical Models

In this paper, we used two methods for the calculation of the THz waveforms. The first method is the one using the Gaussian beam theory, where each frequency component of the THz beam is assumed as a Gaussian beam. In the second method, a simple analytical expression is used, which is derived from the Gaussian beam theory using appropriate approximation. In these methods, the starting field on the surface of the emitter was obtained based on the current surge model, which describes the THz wave generation process at the emitter.<sup>6,12)</sup>

In both of the simulation methods, obtained waveforms were convoluted with a 150 fs Gaussian probe pulse shape in order to incorporate the finite time resolution of the electro-optic sampling detection. Loss of the THz radiation by reflection at surfaces of optical elements was also taken into account in the calculation of the waveforms for the comparison with the experimental ones. The THz pulse was reflected at the rear surface of the emitter GaAs wafer and at the front surface of the ZnTe crystal before the detection. Using the normal incidence reflectivity of 28.9% for GaAs<sup>13)</sup> and 16% for ZnTe,<sup>14)</sup> the overall amplitude reduction of the THz pulses by the reflection was calculated to be 23%.

#### 3.1 Current surge model

The current surge model is widely accepted as the model describing the THz field at the surface of the emitter,<sup>6,12)</sup> which is needed as the starting point of the calculation of the propagated THz waveforms. In this model, the THz electric field on the surface of the emitter is given by

$$E_{\text{surf}}(t) = -E_{\text{bias}} \frac{\sigma_s(t)\eta_0}{\sigma_s(t)\eta_0 + 1 + \sqrt{\epsilon}}. \quad (2)$$

Here,  $E_{\text{bias}}$  is the bias field,  $\sigma_s(t)$  is the time-dependent surface conductivity,  $\epsilon$  is the dielectric constant of the emitter medium, and  $\eta_0 = 377 \Omega$  is the impedance of vacuum. The bias field,  $E_{\text{bias}}$ , was assumed constant through the intergap area in the waveform simulation.

The surface conductivity is given by<sup>6)</sup>

$$\sigma_s(t) = \frac{e(1-R)}{h\nu} \int_{-\infty}^t \mu(t-t') I_{\text{opt}}(t') \exp[-(t-t')/\tau_{\text{car}}] dt'. \quad (3)$$

Here,  $e$  is the elemental charge,  $R$  is the reflectivity of the pump pulse at the emitter surface,  $\mu(t-t')$  is the time-dependent electron mobility,  $I_{\text{opt}}(t')$  is the intensity of the pump pulse, and  $\tau_{\text{car}}$  is the carrier lifetime. The functional form of  $\mu(t-t')$  is

$$\mu(t) = \mu_{\text{dc}} - (\mu_{\text{dc}} - \mu_i) \exp(-\Gamma t). \quad (4)$$

This expression describes the time-dependent mobility of electrons which are excited above the bottom of the conduction band and relax to the bottom with the relaxation lifetime of  $\Gamma^{-1}$ . The pulse shape of the pump light was assumed to be Gaussian as

$$I_{\text{opt}}(t) = I_0 \exp(-t^2/t_{\text{las}}^2). \quad (5)$$

The following parameters were used:  $R = 0.3$ ,  $\epsilon = 12.25$ ,

$\Gamma = 2$  THz,  $\mu_{dc} = 8000$  cm<sup>2</sup>/V·s, and  $\mu_i = 500$  cm<sup>2</sup>/V·s. The value of the carrier lifetime,  $\tau_{car}$ , of 50 ps was adopted instead of 600 ps, which was used by Gürtler *et al.*,<sup>6)</sup> in the simulation in order to speed up the decay of the surface field. This was required since in the Gaussian beam method, the whole waveform of the surface field is needed for the Fourier transformation. The value of carrier lifetime, however, was found to affect the calculated waveforms negligibly in the time window of the present study. The pump pulse duration was modified from the experimental value of 150 fs to an effective pulse width in order to make the simulated THz pulse width consistent with the experimental one, as described in §4. The spatial distribution of the pump pulse fluence was assumed to be Gaussian, which is justified by the experimental observation of the spatial profile of the pump fluence, as described above.

### 3.2 Gaussian beam theory

We modeled the experimental setup on the simplified one shown in Fig. 2. Here, the parabolic mirror is represented by a lens. The lens diameter and the lens focal length are  $D$  and  $f$ , respectively. The  $1/e$  radius of the field amplitude of the THz beam on the surface of the emitter is represented by  $A$ , which is equal to the  $1/e$  radius of the pump pulse fluence distribution. Using this model, we simulated the experimentally observed waveforms based on the Gaussian beam theory, in which each frequency component of the THz pulse is assumed to propagate as a Gaussian beam.

The electric field of a Gaussian beam with frequency  $\nu$  is expressed as<sup>15)</sup>

$$E(x, y, z, t) = E_0 \cdot \frac{w_0}{w(z)} e^{i2\pi\nu t} \times \exp\left[-i(kz - \eta(z)) - r^2\left(\frac{1}{w^2(z)} + \frac{ik}{2R(z)}\right)\right], \quad (6)$$

where  $z$  is the position in the propagation direction,  $k = 2\pi/\lambda$  is the wave vector of the component with wavelength  $\lambda = c/\nu$ , and  $c$  is the speed of light,

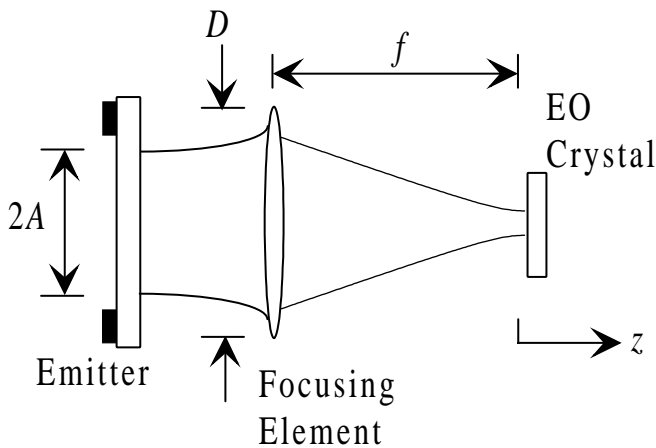


Fig. 2. Model of setup adopted in the theoretical treatment.  $A$  is the beam size at the emitter,  $D$  is the lens diameter, and  $f$  is the focal length of the lens.

$$\eta(z) = \tan^{-1}\left(\frac{z}{z_0}\right), \quad (7)$$

$$z_0 = \frac{\pi w_0^2}{\lambda}, \quad (8)$$

$$w^2(z) = w_0^2\left(1 + \frac{z^2}{z_0^2}\right), \quad (9)$$

$$R(z) = z\left(1 + \frac{z_0^2}{z^2}\right), \quad (10)$$

and

$$r^2 = x^2 + y^2. \quad (11)$$

The refractive index is assumed to be unity. The beam waist is located at  $z = 0$  in this expression.

The THz beam emitted from the large-aperture photoconductive antenna is assumed to be a Gaussian beam. Since the spatial distribution of the pump fluence was observed to be nearly Gaussian, as described in the experimental section, it is a reasonable assumption. The bias field is assumed to be constant through the intergap area. We locate the beam waist at the emitter surface, which corresponds to the experimental condition that the pump beam is collimated at the emitter. The beam size  $w$  is set to be  $A$  at the emitter surface. This beam is made to propagate in the free space between the emitter and the lens according to the Gaussian beam theory. The lens converts the radius of curvature  $R$  to  $R'$  by

$$\frac{1}{R'} = \frac{1}{R} - \frac{1}{f}. \quad (12)$$

The effect of the finite size of the lens of diameter  $D$  is taken into account by assuming that the spatial transmittance profile  $T(r)$  of the lens is expressed by a Gaussian function as

$$T(r) = \exp\left(-\frac{4r^2}{D^2}\right). \quad (13)$$

Here,  $r$  is the distance from the beam propagation axis. Then the beam size  $w$  is transformed to  $w'$  by the transmission through the lens as

$$\frac{1}{w'^2} = \frac{1}{w^2} + \frac{2}{D^2}. \quad (14)$$

The position  $z'_f$  and the size  $w'_0$  of the beam waist of the Gaussian beam transformed by its passage through the lens are calculated using  $R'$  and  $w'$  as

$$z'_f = z_L - R' \left[1 + \left(\frac{cR'}{\pi\nu w'^2}\right)^2\right]^{-1}, \quad (15)$$

$$w'_0 = w' \left[1 + \left(\frac{\pi\nu w'^2}{cR'}\right)^2\right]^{-1/2}. \quad (16)$$

Here,  $z_L$  is the position of the lens. The phase  $\eta$  of each frequency component is maintained at the lens.

In the simulations of the THz waveforms, the surface field waveforms at the center of the emitter were first calculated using eq. (2), and then Fourier transformed. Then each frequency component was assumed to be a Gaussian beam with a field  $1/e$  radius of 9.2 mm, and transformed using the

procedures described above, corresponding to the spatial propagation. The temporal waveforms at the observation points were obtained by inverse Fourier transformation of the frequency-dependent complex amplitude.

### 3.3 Analytical model

In order to obtain a high peak field, THz radiation emitted from the antenna is required to be focused onto a small spot. There has been no theory available for the estimation of the absolute magnitude of the field strength of the focused THz radiation. The expression for the waveform of far-field THz radiation has been obtained.<sup>16)</sup> It shows that the far-field THz waveform is proportional to the time derivative of the surface field waveform. Although the waveform of focused THz radiation should be proportional to the far-field waveform, the proportionality factor has not been derived. A theoretical framework for the estimation of the absolute value of the peak field of focused THz radiation is necessary for the understanding and development of intense THz radiation sources and application of emitted intense THz field in nonlinear experiments.

We simplify the model shown in Fig. 2 to obtain analytical expressions for the focused THz waveforms. Here, a lens is placed close to the THz pulse emitter, and it is assumed that diffraction of the emitted THz beam can be neglected at the lens, and that the beam size at the focusing element is maintained at  $A$  because of the close alignment of the focusing element with the emitter. The EO crystal is positioned at the focus of the lens, and the waveform of the THz radiation at this position is measured.

Radius of the beam at the lens,  $A$ , is given by the expression:

$$A^2 = w^2(-f) = w_0^2 \left( 1 + \frac{f^2}{z_0^2} \right). \quad (17)$$

Now we assume that the major contribution to the THz radiation power is due to the frequency components that satisfy

$$z_0 \ll f. \quad (18)$$

This is equivalent to

$$\lambda \ll \frac{\pi A^2}{f}. \quad (19)$$

Under this condition, eq. (17) is approximated as

$$A^2 = \left( \frac{w_0 f}{z_0} \right)^2, \quad (20)$$

and the phase of the field oscillations at the position of the lens can be approximated as

$$\eta(-f) = -\frac{\pi}{2}. \quad (21)$$

The beam waist size of the component with frequency  $\nu$  is now obtained as

$$w_0 = \frac{cf}{A\pi\nu}. \quad (22)$$

By using this result, electric field amplitudes of  $\nu$  component at the focus and on the emitter surface are expressed as

$$E_{\text{focus}}(\nu) = E_0 \quad (23)$$

and

$$E_{\text{surf}}(\nu) = -\frac{icf}{\pi A^2 \nu} E_0, \quad (24)$$

respectively. Thus, the field amplitude at the focus is related to the amplitude of the surface field as

$$E_{\text{focus}}(\nu) = \frac{i\pi A^2 \nu}{cf} E_{\text{surf}}(\nu), \quad (25)$$

or, in the time domain,

$$E_{\text{focus}}(t) = \frac{A^2}{2cf} \frac{d}{dt} E_{\text{surf}}(t). \quad (26)$$

This expression shows that the focused waveform is proportional to the time derivative of the surface field waveform as expected. Furthermore, this is, to the authors' knowledge, the first derivation of the expression which relates the magnitude of the waveforms of focused THz field to the surface field waveforms. This expression can be used not only for the study of the waveforms of a focused field but also for estimation of the absolute value of possible peak field under the experimental setup used.

## 4. Results and Discussion

Experimentally obtained waveforms are shown in Fig. 3. The ZnTe crystal was moved along the axis of the THz beam propagation from the focus,  $z = 0$  mm, to 50 mm away from the focus. Waveforms at every 10 mm are shown in the figure. Since the probe pulse propagates collinearly with the THz beam, the time origin also moves at the speed of light along the  $z$  axis. By increasing  $z$ , it was observed that the peak was lowered, the pulse was broadened, and the peak position was shifted in the negative direction.

The broadening and the peak reduction can easily be understood using the Gaussian beam model. Each frequency component of the THz radiation can be approximately regarded as propagating like a Gaussian beam. The beam waist size  $w_0$  of the Gaussian beam is inversely proportional to the frequency as shown in eq. (22), and the confocal parameter  $z_0$ , which represents the length of the beam waist, is also inversely proportional to the frequency. Thus, higher frequency components are focused more tightly and expand

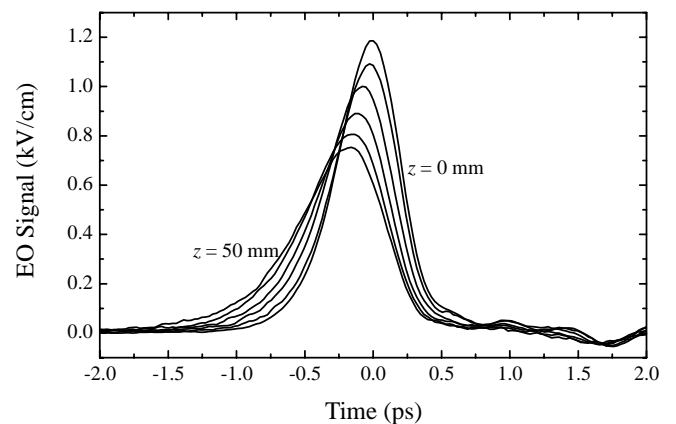


Fig. 3. Experimentally obtained waveforms of the THz pulses at positions from  $z = 0$  mm to  $z = 50$  mm in steps of 10 mm.

faster than lower frequency components. When the THz pulse travels away from the focus, the spectrum becomes narrower because of the faster reduction of higher frequency components, which leads to a broadening of the pulse. At the same time, the amplitudes of components of all frequencies are reduced, which results in the reduction of the amplitude of the temporal waveform.

The peak shift which was observed in the experiments is explained by the following consideration. The time origin of each waveform is determined based on the optical path length of the on-axis ray. Path lengths of off-axis rays are equal to that of the on-axis ray at the focus, and shorter than that of the on-axis ray at a position away from the focus. Thus at positions farther away from the parabolic mirror than the focus, the off-axis contribution of the pulse arrives faster than that of the on-axis ray. In pulses which contain many cycles of field oscillations, such as femtosecond optical pulses, off-axis contributions cancel out because of destructive interference among them, and only the on- and near-axis rays contribute to the waveform observed at positions on the propagation axis. This is the consequence of Fermat's principle that optical rays take the path of minimal path length. Fermat's principle, however, is only valid within the limit of the geometric optics, and it can fail for half-cycle pulses, which contain a significant portion of low-frequency components. THz pulses generated using femtosecond optical pulses can be nearly half-cycle, and have a very broad spectrum extending from dc to a few THz. This causes the pronounced pulse broadening and shift as observed in the experiment and the simulation.

Fourier amplitudes of the waveforms observed are shown in Fig. 4. The oscillations in the spectra are caused by a sub-peak observed at 8.5 ps after the main peak in the waveform, which is a reflection of the main pulse by the surfaces of the emitter. By increasing  $z$ , the Fourier amplitude becomes smaller. The decrease is faster at components of higher frequencies. It is consistent with the trend observed in the temporal waveforms.

In the simulation calculation, we used the current surge model to describe the generation process of the THz pulses as described in the previous section. The pulse shape of the pump pulse was assumed to be Gaussian. It was found that

simulated waveforms using a pump pulse width of the experimental value of 150 fs were much shorter than those experimentally observed. For example, the pulse width (full-width at half maximum) of the simulated waveform at the focus using the Gaussian beam method was 350 fs, and that of the experimental one was 530 fs. This is probably because the model of the carrier dynamics used in the simulation is not appropriate. High-density carriers are created in the emitter in the experimental condition for intense THz pulse generation. Because the simple dynamical model described in the previous section is based on the carrier dynamics at a low excitation level,<sup>17)</sup> it is reasonable that it cannot be applied under actual experimental conditions. Since it is not the purpose of the present study to elaborate the dynamical model of the generation processes, we adopted an effective pump pulse width of 364 fs instead, and obtained good agreement between the experimental THz pulse width and that simulated by the Gaussian beam method.

The waveform at the focus obtained by the Gaussian beam method using this value of the effective pump pulse width is shown in Fig. 5 with the experimentally observed one. It is seen from the figure that although the pulse durations of the experimental waveform and that of the Gaussian beam method agree well with each other, there is a difference in the pulse shape. The simulated waveform rises faster than the experimental one, and decays more slowly with an exponential tail. On the other hand, the experimental waveform is almost symmetrical. This waveform suggests that the relaxation of the hot carriers to the quasi-equilibrium state occurs faster in the experimental condition than under low excitation. In the present paper, however, we will use this model of the dynamics of the photoexcited carriers with the effective pump pulse width of 364 fs, and focus on the general trends of the waveform transformation of the THz pulses through the propagation around the focus.

Furthermore, a close look at the figure shows that the peaks of the Gaussian beam waveform and the experimental one do not coincide with each other. In the figure, the time origin of the experimental waveform is set at the peak. On the other hand, the time origin of the simulated waveform is set at the time when the peak of the pump pulse should reach the observation point if the emitter were to be removed from

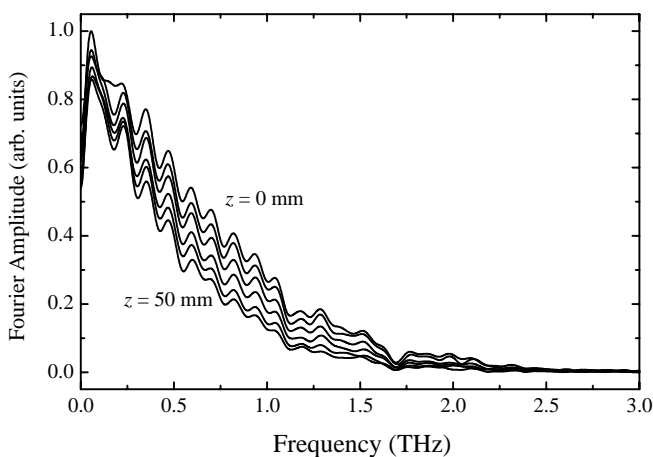


Fig. 4. Fourier amplitudes of the experimentally obtained waveforms. The observation points were at  $z = 0$  mm to  $z = 50$  mm in steps of 10 mm.

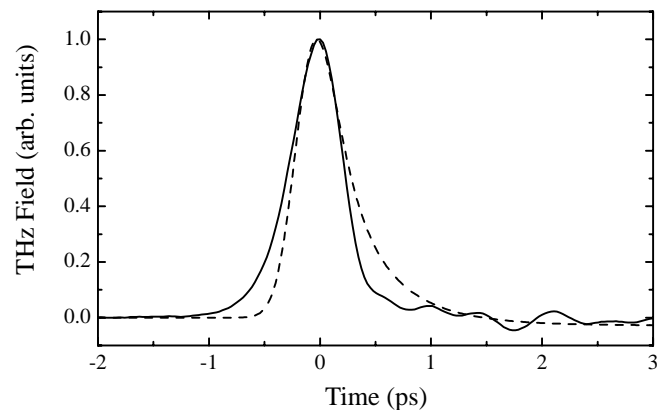


Fig. 5. Normalized waveforms at the focus obtained in the experiment (solid line) and by the simulation based on the Gaussian beam method (dashed line). An effective pump pulse width of 364 fs was used for the simulation.

the experimental setup. The small shift of the peak of the waveform of the Gaussian beam simulation in the negative time direction is attributed to a saturation effect as explained below. When the saturation fluence for the pump pulse,  $F_{\text{sat}}$ , is defined by<sup>3)</sup>

$$F_{\text{sat}} \equiv \frac{h\nu(1 + \sqrt{\epsilon})}{e\mu_{\text{dc}}\eta_0(1 - R)}, \quad (27)$$

the value of the pump fluence at the emitter center used in the present study,  $3.6 \mu\text{J}/\text{cm}^2$ , is slightly above the saturation fluence  $F_{\text{sat}} = 3.3 \mu\text{J}/\text{cm}^2$ . When the pump fluence is large, the current density on the emitter surface is saturated in the current surge model, and the resultant waveform of the focused THz pulse is affected as follows: (i) the peak field magnitude is saturated, (ii) the peak time is shifted in the negative direction, and (iii) the pulse width is narrowed. Simulations for these effects have been reported in the previous paper.<sup>3)</sup> The time shift of the Gaussian simulation result corresponds to the mildly saturated fluence level in the present study.

Waveforms from  $z = 0 \text{ mm}$  to  $z = 50 \text{ mm}$  obtained by the Gaussian beam method are shown in Fig. 6. General trends of the simulated data show good agreement with those obtained in the experiments. The obtained waveforms show a peak shift in the negative direction of time, amplitude decrease, and broadening, as the observation position  $z$  is increased.

The position dependence of the pulse width is plotted in Fig. 7 for a quantitative comparison of the results of the experiments and the simulation. The experimental and simulation results agree well when  $z \leq 20 \text{ mm}$ . This shows that the Gaussian beam model can describe well the THz wave propagation near the focus. The experimental results start to deviate from the Gaussian beam results when  $z$  becomes larger than  $20 \text{ mm}$ . The difference in the pulse width between the experimental and the Gaussian beam waveforms is about 10%  $50 \text{ mm}$  from the focus.

An interesting point seen in the position dependence of the experimental results is that the pulse width at  $z = 5 \text{ mm}$  is slightly smaller than that of the simulation result. This can also be explained by taking into account the saturation effect. Since the surge current in the central area of the

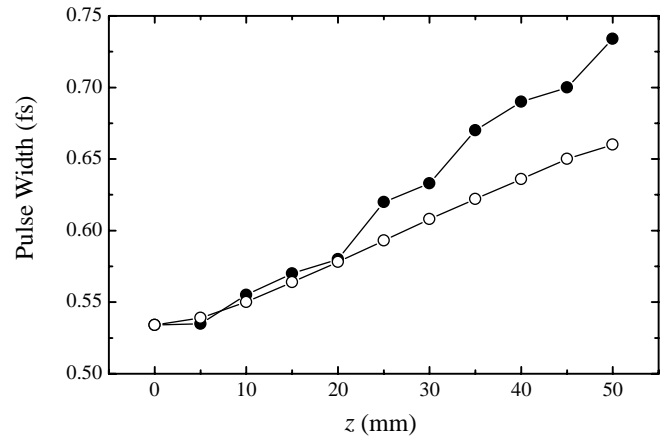


Fig. 7. Pulse widths (full-width at half maximum) of the THz waveforms as a function of the observation position  $z$ . Black circles show the experimental values and open circles show those of the Gaussian beam simulation.

emitter surface is most saturated, the THz pulse emitted is slightly temporally advanced at the center. This is equivalent to the case where the THz pulse is slightly divergent at the emitter surface, which makes the beam waist position slightly farther than the focus. This position-dependent saturation effect is not taken into account in the Gaussian beam simulation. In the simulation, the surface field at the center of the emitter is calculated by the current surge model. The THz pulse radiated from the emitter surface is assumed to have a Gaussian spatial profile with the same temporal waveform corresponding to this surface field at each position.

In order to test the validity of the analytical expression of eq. (26) for the THz waveform at the focus, the waveform at the focus obtained using this equation is plotted in Fig. 8 with those obtained in the experiment and the Gaussian beam simulation without amplitude normalization. The amplitudes of the simulated waveforms agree well with each other. The experimental waveform has an amplitude of about 60% of the simulated ones. The discrepancy is probably due to the error in the evaluation of the magnitude of the field amplitude in the EO sampling detection. Since the EO constant of ZnTe crystals depends on the crystal

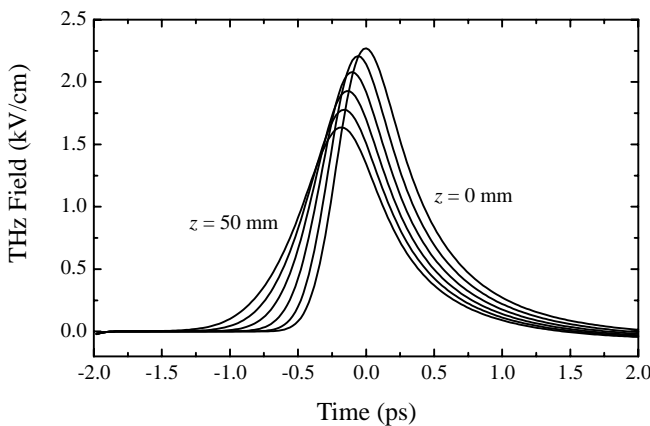


Fig. 6. Waveforms obtained by the simulation based on the Gaussian beam method. The observation points were at  $z = 0 \text{ mm}$  to  $z = 50 \text{ mm}$  in steps of  $10 \text{ mm}$ .

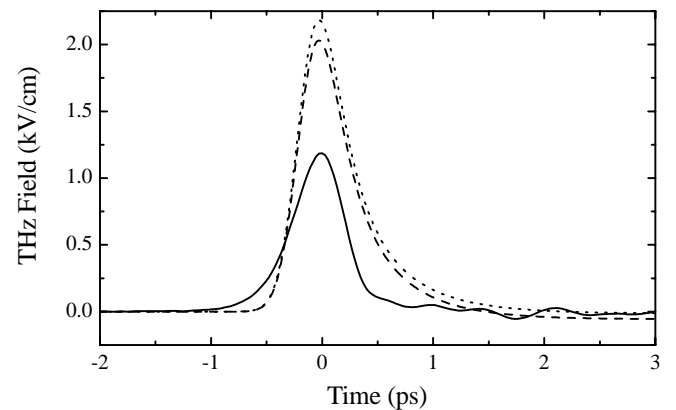


Fig. 8. THz waveforms at the focus obtained in the experiment (solid line), by the Gaussian beam simulation (dashed line), and by the analytic expression (dotted line).

quality, the EO constant of the actual crystal can be smaller than the literature value. In any case, this can be regarded as being good agreement since there is no adjustment parameter. It can be concluded that the simple analytical expression can be used to predict the waveforms and the magnitude of the THz pulses at the focus fairly well.

From the expression for the waveform of focused THz radiation obtained in the present study, eq. (26), we can roughly estimate the highest peak field that can be achieved by focusing THz radiation emitted by large-aperture biased emitters. Since the surface field switches on from zero to a value almost equal to  $E_{\text{bias}}$  in the duration of the effective pump pulse width under saturated conditions, the achievable peak electric field is estimated as:

$$E_{\text{peak}} \approx \frac{A^2}{2c\tau_{\text{eff}}f} E_{\text{bias}}. \quad (28)$$

Here, the value of  $\tau_{\text{eff}}$  is 364 fs for GaAs emitters in the present study. This relation is simple and useful for the design of the setup for intense THz field generation for a specific purpose. For example, by using parameters of the present experimental conditions, it is calculated that the peak field achievable under saturated conditions is  $E_{\text{peak}} \approx 2.5E_{\text{bias}}$ .

## 5. Conclusions

Temporal waveform transformation of THz pulses around the focus was observed experimentally. The THz pulse was generated by a large-aperture photoconductive antenna. The results were compared with waveforms simulated by the Gaussian beam method. It was found that the Gaussian beam simulation can describe the waveform transformation of THz pulses around the focus. A simple analytical expression describing the waveform and the magnitude of the THz field at the focus was also derived, and the calculated waveform was found to agree very well with those obtained by the

Gaussian beam simulation. In the experiment, a spatial beam waist shift was observed, which was attributed to the position-dependent saturation of the surge current on the emitter surface in the THz pulse generation process.

## Acknowledgements

This study was partly supported by the Research Foundation for Opto-Science and Technology, and by the Grant-in-Aid for Scientific Research from the Japan Society for Promotion of Science.

- 1) D. You, R. R. Jones, P. H. Bucksbaum and D. R. Dykaar: *Opt. Lett.* **18** (1993) 290.
- 2) E. Budiarto, J. Margolies, S. Jeong, J. Son and J. Bokor: *IEEE J. Quantum Electron.* **32** (1996) 1839.
- 3) T. Hattori, K. Tukamoto and H. Nakatsuka: *Jpn. J. Appl. Phys.* **40** (2001) 4907.
- 4) D. You and P. H. Bucksbaum: *J. Opt. Soc. Am. B* **14** (1997) 1651.
- 5) K. Tukamoto, R. Rungsawang and T. Hattori: in preparation.
- 6) A. Gürtler, C. Winnewisser, H. Helm and P. U. Jepsen: *J. Opt. Soc. Am. A* **17** (2000) 74.
- 7) E. Budiarto, N.-W. Pu, S. Jeong and J. Bokor: *Opt. Lett.* **23** (1998) 213.
- 8) K. Tukamoto, R. Rungsawang, T. Fujii and T. Hattori: in preparation.
- 9) A. Nahata, A. S. Welington and T. F. Heinz: *Appl. Phys. Lett.* **69** (1996) 2321.
- 10) T. R. Sliker and J. M. Jost: *J. Opt. Soc. Am.* **56** (1966) 130.
- 11) D. T. F. Marple: *J. Appl. Phys.* **35** (1964) 539.
- 12) J. T. Darrow, X.-C. Zhang, D. H. Auston and J. D. Morse: *IEEE J. Quantum Electron.* **28** (1992) 1607.
- 13) H. R. Philipp and H. Ehrenreich: *Phys. Rev.* **129** (1963) 1550.
- 14) J. P. Walter, M. L. Cohen, Y. Petroff and M. Balkanski: *Phys. Rev. B* **1** (1970) 2661.
- 15) A. Yariv: *Quantum Electronics* (Wiley, New York, 1988) 3rd ed., Chap. 6.
- 16) P. K. Benicewicz, J. P. Roberts and A. J. Taylor: *J. Opt. Soc. Am. B* **11** (1994) 2533.
- 17) M. C. Nuss, D. H. Auston and F. Capasso: *Phys. Rev. Lett.* **58** (1987) 2355.